

Article

Mineralogy, Geochemistry and Fluid Inclusion Data from the Tumanpinarı Volcanic Rock-Hosted Fe-Mn-Ba Deposit, Balıkesir-Dursunbey, Turkey

Ali Haydar Gultekin * and Nurgul Balcı

Jeoloji Muhendisligi Bolumu, Maden Fakultesi, Istanbul Teknik Universitesi, Maslak 34469, Istanbul, Turkey; ncelik@itu.edu.tr

* Correspondence: ahgultekin@hotmail.com; Tel.: +90-212-285-6119

Academic Editor: Maria Economou-Eliopoulos

Received: 27 July 2016; Accepted: 31 October 2016; Published: 4 November 2016

Abstract: The Tumanpinarı mineralization is a volcanic rock-hosted epithermal Fe-Mn-Ba deposit located in the southwestern part of Dursunbey, Balıkesir, Turkey. The deposit constitutes one of the most important deposits of the Havran-Dursunbey metallogenic sub-province in which numerous Early Miocene Fe-Mn-Ba deposits are distributed. The ore occurs as open-space fillings in faults, fractures, and breccias in the andesite. Early hydrothermal activity was responsible for four types of hypogene alteration in decreasing intensity: silicification, sericitization, hematization and argillic alteration. The mineral assemblage includes pyrolusite, psilomelane, hematite, and barite as well as minor magnetite, manganese, poliamnite, limonite, braunite, bixbyite, galena, pyrite, and goethite. Mineralogically, three ore types are recognized as pyrolusite + psilomelane + hematite + barite ore, pyrolusite + psilomelane + poliamnite ore and barite + pyrolusite + psilomelane + hematite ore (barite-dominant ore). In addition to Fe, Mn and Ba, the ore contains substantial quantities of Pb, Zn, As. Chemically, the transition from fresh to altered rocks has little effect on the elemental levels for Si, Al, Fe, Ca, Mg, K, Rb, Sr and H₂O. The homogenization temperature of fluid inclusions hosted in the main stage quartz and barite ranged from 113 to 410 °C with salinities ranging from 0.4 to 14.9 eq. wt % NaCl, respectively. Overall, the available data suggest that the deposits formed as the result of the interaction of two aqueous fluids: a higher-salinity fluid (probably magmatic) and a dilute meteoric fluid.

Keywords: ore; alteration; magmatic fluid; hydrothermal; andesite

1. Introduction

The Tumanpinarı Fe-Mn-Ba ore deposit, hosted in Miocene andesitic rock, is located approximately 30 km SW of the town of Dursunbey, Balıkesir province, NW Anatolia (Figure 1A,B). The deposit is one of the most important mines in the Havran-Dursunbey sub-province of the northwestern Anatolian metallogenic province (Figure 1C). The sub-province is one of the most productive district for base and precious metals in addition to its industrial minerals (e.g., clays) in Turkey. There have been almost 30 separate Fe-Mn ± Ba occurrences recorded around this sub-province. The mining history of the Havran-Dursunbey goes back to ancient times where the mine was used to provide the first known lead, gold and iron products to nearby Troy [1].

Numerous research has been conducted in the western Anatolia metallogenic province, focusing mainly on the geology and mineralogy of the deposits [2–6]. The economically significant deposits in the province are related to calc-alkaline magmatism which was extensively studied by Yilmaz (1990) [7] and Ercan et al. (1985) [8]. The close association of Mn-Fe-Ba deposits with calc-alkaline volcanism in northwestern Anatolia was first described in detail by Gultekin et al. (1998) [9,10].

The authors were proposed that the deposits were formed under the epithermal conditions and further explained the paragenesis in detail. Most extensive data on the metallogenic history and exploration potential of the district can be found in Yigit et al. (2012) [11]. The recent research on the deposits has been conducted by the General Directorate of Mineral Research and Exploration (MTA). In the Tumanpinarı deposits, from 25 boreholes totaling 960 m in length, the MTA identified a geological reserve of approximately 1.0 Mt grading at 27.98% Fe₂O₃, 22.40% MnO and 38.02% BaO consistent with the previous studies reporting an average 2.7% Pb and 0.1% Zn [2]. Although a significant amount of research was conducted in the region, the origin and chemistry of hydrothermal liquids that caused the formation of the Tumanpinarı deposits have not been sufficiently discussed. Most of these studies only suggested a hydrothermal origin for the deposits but did not provide in detail the temperature ranges, paragenesis and chemistry of hydrothermal fluids that created the deposits. Since the district is newly recognized for precious metals (e.g., Au), potential new insights and re-evaluation of the origin of the deposits can provide valuable information for prospection.

The purpose of this paper is to determine the source of metals, sulfur, and the hydrothermal fluids involved in the genesis of the Tumanpinarı deposit. The ore mineralogy, geochemistry, sulfur isotopes and fluid inclusions data were used to determine the origin of the ore forming fluids and to elucidate the genesis of the manganese-iron-barium veins and the Tumanpinarı hydrothermal system. The results presented in this study may provide a useful guide for the exploration of similar ore deposits in the region.

2. Geology

The rock outcropping in the Havran-Dursunbey district and near vicinity range from Paleozoic to Tertiary in age (Figure 1D,E). The volcanic rocks of the Cenozoic age are the most common rocks and seem to be the product of calc-alkaline volcanic affinity that is associated with the closure of the Tethys Ocean [7,12–19].

The Paleozoic basement rocks consist of quartz-albite-muscovite schists, quartz-albite-sericite-chlorite schist, calc-schists, and quartzites which lie within a broad area of metamorphic rocks. This basement is conformably overlain by the Upper Paleozoic metasedimentary rocks in the western part of Dursunbey district. The metasedimentary rocks are represented mainly by greywacke with a limestone interlayer of several meters thick and tectonically in contact with the ophiolitic complexes. The Mesozoic sequence in the region starts with basal conglomerates, sandstones, and claystones overlaying unconformably on the Paleozoic metamorphic rocks. The deposition of this initial formation of the Mesozoic sequence was followed by the Jurassic formation consisting mainly of recrystallized limestones. The latter recrystallized limestones are characterized by the Pb, Zn deposits of skarn type formed in contact with the younger granitoids, especially granodiorite. The deep wine colored limestones and ophiolitic mélange of the Cretaceous age form the upper unit of the Mesozoic sequence.

The Tertiary sedimentary formations consist mainly of limestone, marl, sandstone, and claystone and represent a regressive sequence developed possibly throughout Eocene. They are covered by the products of widespread post-Oligocene volcanism that began during Late Oligocene–Early Miocene in a compressional regime [7]. The Tertiary units also consist of Neogene tuff with a yellowish-gray limestone interlayer that formed a lacustrine basin. The post-Oligocene volcanism resulted in a widespread suite of calc-alkaline rocks, consisting mainly of andesite, latite and dasite. The abrupt change from N-S compression to N-S stretching in the Middle Miocene was accompanied by a gradual transition to alkali basaltic volcanism [18]. The calc-alkaline volcanic rocks host the many types of hydrothermal veins in the Balikesir-Dursunbey region.

The Tumanpinarı ore veins, the focus of this study, are associated with andesite, a product of the post-Oligocene volcanism (Figures 1E and 2). Andesites in the study area are dark yellow and brown, fine-to coarse-grained rocks, composed of plagioclase, amphibole, biotite and volcanic glass, lesser chlorite, epidote, and sanidine microlites, and mostly display the hyalocrustalline porphyritic texture. Plagioclases occur as oligoclase and andesine phenocrystals in a finer-grained groundmass

and glassy material. Early hydrothermal activity that leads to a hypogene alteration in the andesite is responsible for the sericitization and argillisation of the plagioclase. Amphiboles are mainly composed of hornblende and are slightly altered to epidote. In the Dursunbey andesite, average modal contents for plagioclase, biotite and amphibole are 53%, 7% and 3%, respectively. Chlorite was observed as a product of the alteration of the amphibole and biotite. On a regional scale, the epidote formation is less obvious in the andesites. They also contain accessory minerals such as magnetite, apatite rutile and zircon.

The Dursunbey district is transversed by a system of closely spaced normal faults. The faults can be grouped into different systems: Faults of the first system strike roughly north-south and dip steeply, generally to the west. The faults of a second system strike about N 30° W and dip to the southwest. The fault systems define the geometry of the Fe-Mn-Ba deposits and the majority of Mn-Fe-Ba deposits appears to be related to these faults. Generally, the tectonic setting was ideal for the movement of hydrothermal solutions along structurally controlled paths towards mineralization.

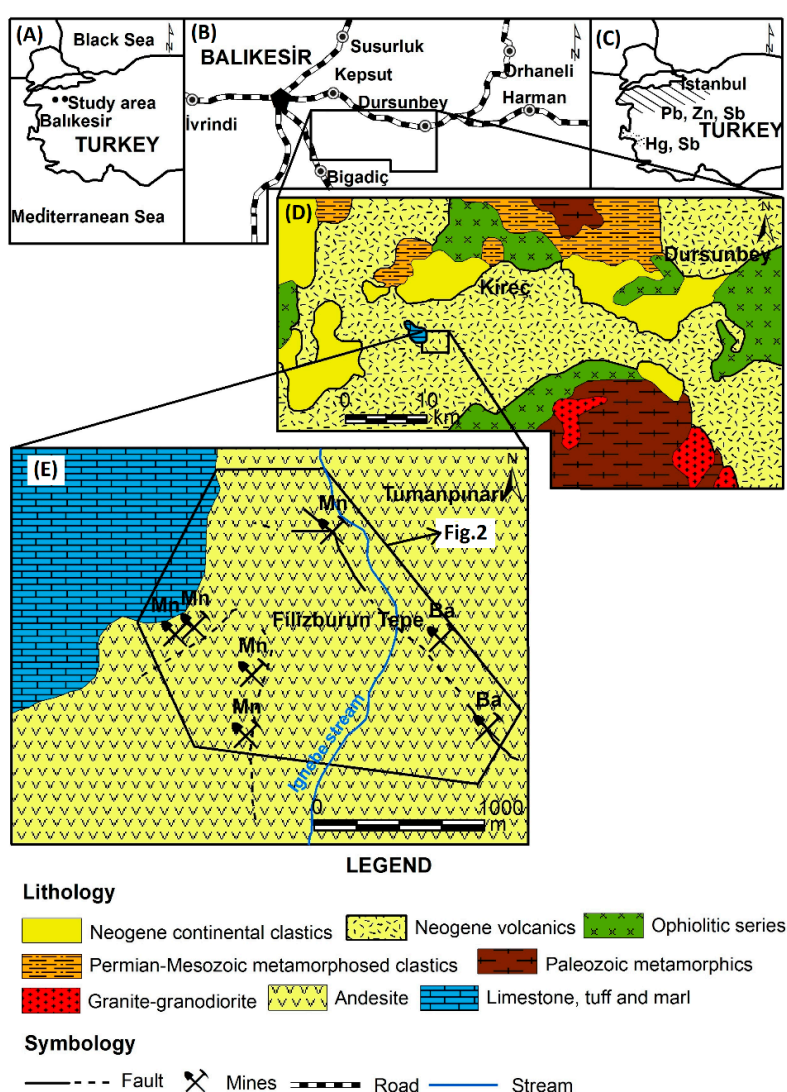


Figure 1. (A,B) Location of the study area; (C) The Alpine metallogenetic units in northwestern Turkey; (D) General geological map of the Balikesir-Dursunbey region [19]; (E) Geological map of the Tumanpinarı mineral area.

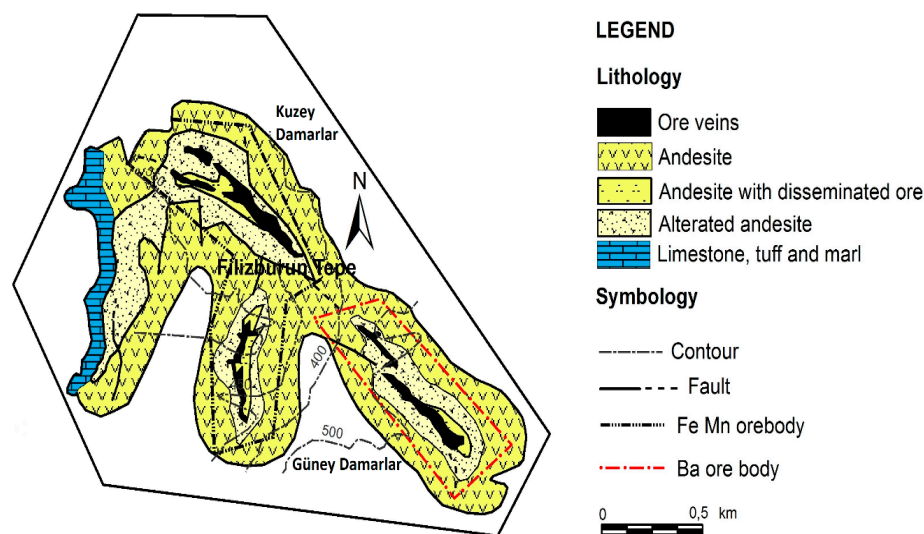


Figure 2. Local geological map of the study area, showing the ore veins, altered and unaltered andesite.

3. Methodology

One hundred and twenty samples were collected from two different levels of the open-pit Fe-Mn-Ba veins as well as from the surface outcrops of the volcanic rocks. Approximately half of the samples ($n = 62$) represent the ore veins ($n = 27$ from barite-dominant ore, $n = 35$ from the Fe-Mn ore), and the rest was taken from the limestones and andesites.

Geochemical samples representing the andesites were taken from fresh exposures as well as from many different outcrops that were altered and contained secondary quartz, clay minerals (i.e., montmorillonite, illite, kaolinite), sericite and chlorite. Following petrographic and ore microscopic studies, 30 representative samples from the fresh and altered andesite were analyzed after crushing in an agate mortar to 325 mesh.

The mineralogical studies are based on X-ray diffraction (XRD), using a Philips diffractometer, with a Cu K α radiation and the thin sections prepared from the ore samples. The two methods are combined for main ore minerals. However, identification of minerals with low content is entirely based on thin sections.

The element contents of the host rocks, and the ore veins were determined at the ACME Analytical Laboratories Ltd. (Vancouver, BC, Canada) by Inductively Coupled Plasma Emission Spectrometer (ICP-ES), using standard G-2 and C13. Detection limits (ppm) were: Lu (0.05); Sm, Ta (0.1); Eu, Yb (0.2); U (0.5); Sc, Cs, Hf (1); V, As, Cr, Co, Ni, Sr, Y, Zr, Nb, La, Th (2); Ce (3); Pb (5); Rb (15). The measurement of the fluid inclusion was made in the Laboratories of the General Directorate of Mineral Research and Exploration (MTA). Fluid inclusion in $\leq 200 \mu\text{m}$ -thick doubly-polished wafers of hydrothermal quartz and barite were studied using standard techniques [20–22] and a Linkam THM600 heating-freezing stage mounted on a Leitz microscope stage. The accuracy is estimated to be $\pm 0.2^\circ\text{C}$ on freezing, $\pm 0.2^\circ\text{C}$ below 350°C and about ± 4 above 350°C on heating. The stage was calibrated at low temperatures with heptane (-90.6°C), chloroform (-63.0°C), chlorobenzene (-45.6°C), *n*-dodecane (-9.6°C) and distilled water (0.0°C). Calibration at 45°C was made with Merck melting point standard 9645, and 306°C with sodium nitrate. In total, 32 doubly polished wafers from the Fe-Mn and barite-dominant samples were prepared for fluid-inclusion studies. However, some of the samples were not suitable for the study because of the fine grain size and abundance of decrepitated inclusions. Heating and freezing measurements were carried out for fluid inclusions in 13 samples of quartz and 11 samples of barite. The samples of quartz are from the pyrolusite + psilomelane + hematite + barite ore from within the core of the orebody. Only two samples of quartz represent the core of the barite-dominant orebody. Over 150 inclusions were measured for temperatures of homogenization

(Th) and 62 for salinity determination. In an attempt to attain reliable data for micro-thermometry, temperatures of homogenization (Th), first ice melting (Te), and last ice melting temperatures (Tm ice) were measured. The temperature determination was performed three times on each inclusion, and the difference between temperature readings of repeated measurements in the same inclusion typically was $<1.0\text{ }^{\circ}\text{C}$. The temperature of homogenization was reported uncorrected for pressure, and was presumably close to the formation temperature, because the ore occurred as open-spaced and fractured fillings at shallow depths.

For sulphur isotope measurements, a total of 13 samples (9 barite and 4 pyrite samples) were used. The samples were crushed with mortar and pure minerals were separated following the methods of Balci et al., 2010 [23] and Schroll and Rantitsch, [24]. The S isotopic composition of the barite and pyrite from the ore veins was determined at the Isotech Laboratories (Champaign, IL, USA). The sulfur isotope results are expressed relative to Vienna Canyon Diablo Troilite (V-CDT), using the standard δ notation:

$$^{34}\delta [\text{‰}] = [(R_{\text{sample}}/R_{\text{standard}}) - 1] \times 10^3$$

where R is the $^{34}\text{S}/^{32}\text{S}$ ratio of sample and standard. The accuracy estimated to be $\pm 0.2\%$ or better.

4. Results

4.1. Hydrothermal Alteration

The field observations and evidences along with the textural and mineralogical data revealed the presence of some alteration zones. The mineralogy and associated mineral abundance of the different types of alteration are given Table 1. In the Tumanpinari area, hydrothermal activity caused four types of wall-rock alterations in decreasing intensity: silicification, sericitisation, hematitisation and argillisation (Figure 3). The andesites were partly altered at the time of their deposition; later, at the time of mineralization and during subsequent weathering. Thus, multiple mineralization events tend to obscure simple zonal alteration patterns. There is a combination of hypogene, hydrothermal and supergene alteration. Nevertheless, hydrothermal alteration is clear in the andesites, affecting an area of about 5 km^2 with a general zonation pattern.

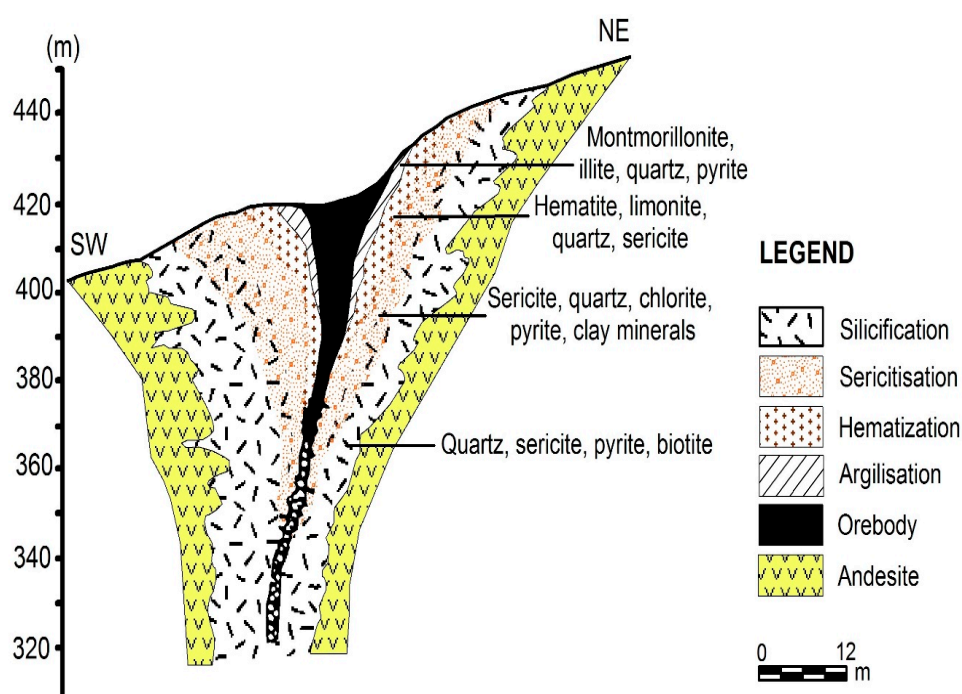


Figure 3. Hydrothermal alteration zones at the Tumanpinari deposit.

Table 1. Mineralogy of the different types found at Tumanpinari.

Alterations	Minerals	Abundance of Minerals			Remark
		Common	Moderately Abundant to Rare	Trace	
Silicic	Quartz	+			Most common alteration types in the andesite as mostly massive and vuggy silica bodies. Presence of different grain-sized quartz. Local hydrothermal quartz crystals in fractures and pores of residual silica. Massive silica consists of microcrystalline quartz derived from the recrystallization of amorphous silica. Occurrence of rutile related to decomposed biotites.
	Sericite		+	+	
	Pyrite			+	
	Biotite			+	
	Chlorite				
Sericitization	Sericite	+			It is seen as a low-intensity alteration haloes surrounding the veins. With progressive alteration, the plagioclase becomes riddled with flakes of fine-grained sericite. Grading outward into silicic alteration.
	Quartz		+		
	Clay minerals (Kaolinite)		+		
	Chlorite			+	
	Pyrite			+	
Hematisation	Hematite	+			The slight reddening of plagioclase and transformation of biotite to chlorite is common. It is seen as haloes surrounding the veins. Some of the hematite is related to ore-stage and shows a textural relationship with magnetite and euhedral quartz crystals.
	Limonite		+		
	Quartz		+		
	Sericite		+		
	Biotite			+	
Argillic	Montmorillonite (Illite)	+			It is seen as a moderate-intensity alteration zone surrounding the massive silica and ore bodies, but locally overprinting the sericitization and hematisation. It is mostly seen as an outer alteration zone and mainly characterized by the complete replacement of plagioclase by clay minerals.
	Quartz	+			
	Pyrite			+	
	Sericite			+	
	Calcite		+		

At Tumanpinari, the ore veins cross-cut the zone of alteration and fractures filled with ore minerals within the silicic breccia matrix. The textural relationships between ore-stage quartz and Mn-oxides, and the presence of feldspar with fine-grained sericite in the veins, are good indications of ore-stage hydrothermal alterations. Silicification is represented by the massive and vuggy silica bodies of microcrystalline quartz, and observed together with hematization towards the ore veins, that is widespread, both on the surface and at depth. The presence of the different grain-sized quartz, secondary pyrite and rutile, related to the decomposed biotites, seems to be the most important evidence of this type of alteration. The silicified zone together with the sericitisation reaches a length of about 3 km in the north-south direction. In the Tumanpinari area, hematization is marked by discoloration of biotite and usually consists of hematite, quartz, limonite, sericite, and a lesser amount of biotite. The plagioclases belonging to this alteration zone show a light reddish color in their fractures and cleavages. The sericitic alteration with a 2.5 km length and roughly 100 m width grades outward into the silicic alteration is represented by sericite, quartz, clay minerals, pyrite and chlorite. These alteration products can be found as far as 20 m from the massive ore. Argillic alteration led to the crystallization of illite and montmorillonite and the bleaching of the rock. In general, argillisation is marked by the complete replacement of plagioclase by these clay minerals, and mostly occurs at contact between massive ore and altered rock and observed in an area of roughly 1 km length.

4.2. Ore Geology

The ore occurs as open-space fillings in faults, fractures, and breccias in the andesite. The deposit mainly contains vein-type formations, but disseminated ore types were also observed in small amounts. The vein-type occurrences entirely show the massive character and their lengths vary between 200 and 1100 m with an average width of 20 m. The geometry of the Fe-Mn-Ba veins are mainly defined by the fault systems and their orientations are parallel to roughly north-south trending regional faults. At the intersections of the faults, the thickness of the orebodies is markedly increased and the thick breccia zones are developed, especially to the north.

The Tumanpinari ore consists of two separate mineralized areas in which the proportions and textures of the major oxides and barites are similar on the local scale. In both areas, the concentrations of ore minerals are suitable for merit production. From northwest to southeast, they are called Kuzey Damarlar and Güney Damarlar areas (Figure 2). The most commercially-important veins related to manganese ore are in the Kuzey Damarlar area. In this area, the mineralization partly occurs in vuggy silica and massive silica bodies within the breccia zones. The Güney damarlar area is distinguished by the occurrences of richer barite.

The mineralogy of the deposits is relatively simple, with the main ore minerals being pyrolusite, psilomelane, hematite and barite which constitute more than 90% of the total ore assemblages. Quartz, magnetite, limonite, manganite, polianite, calcite, manganocalcite, goethite, galena, pyrite, braunite, bixbyite and clay minerals, in decreasing order of abundance, are other members of the Tumanpinari mineral assemblages. Pyrolusite is the most abundant manganese mineral, varying from 10 to 60 wt %, and mostly occurs together with other manganese minerals such as psilomelane and manganite. The pyrolusite typically seems to be as subhedral to anhedral grains in the ore veins and the fault zones, occasionally as pyrolusite masses adjacent to barite grains and in massive silica bodies. Some pyrolusite-rich veins are cut by veinlets containing pyrolusite, psilomelane and hematite. Similarly, massive pyrolusite is also cut by the fine barite veins in many places. Psilomelane, mostly subhedral grains, is less abundant than pyrolusite and occasionally forms individual dark-colored bands. This mineral is mainly associated with high-grade ore veins. Hematite typically occurs as fine-grained radial or prismatic crystals, with concentrations varying from 8 to 30 wt %. In some places, hematite occurs as massive fracture fillings with magnetite and limonite. Barite is mostly observed as subhedral and anhedral crystals up to 10 mm in length, sometimes intergrown with other manganese and iron minerals or occurring in small cavities within it. Locally, pyrite crystals occur in the fractures in the vuggy silica and massive silica bodies, but is generally finer grained

and granular, comprising less than 2% of the vein fill. Late quartz and calcite crystals line cavities and are coated with black, smooth manganese and iron oxides. Limonite and goethite are mainly associated with supergene alteration. The mineralogical studies have revealed the presence of minor Mn-bearing phases associated with the main ore phases such as pyrolusite, psilomelane and manganite. These Mn-bearing phases are poliannite, braunite, bixbyite and manganocalcite. These minerals have not been recognized, so far, in hand specimen, but in the thin and especially polished section, and occurs as accessory minerals. Galena is the most abundant sulphide mineral, varying from 0.5 to 3.0 wt %. It occurs as isolated subhedral to anhedral grains, especially in the Fe-Mn oxide veins with pyrite. Except the main ore minerals, the other Fe-Mn minerals cannot be described in detail due to their low contents and fine grains.

On the basis of the predominant minerals, the veins deposits can be divided into three different parageneses: (1) Pyrolusite + psilomelane + hematite + barite ore; (2) Pyrolusite + psilomelane + poliannite ore; (3) Barite + pyrolusite + psilomelane + hematite ore (barite-dominant ore). However, each paragenesis also contains the other oxides and gangue minerals in varying amounts. Generally, the parageneses (1) and (3) are predominant. The occurrences and textures of ore minerals are entirely similar in all types of mineralization. Their amounts, however, show some differences in the veins.

The Pyrolusite + psilomelane + hematite + barite is the most common paragenesis, with a vertical extension of at least 40 m. This type of mineralization occurs in north-and northwest-trending veins, which follows the faults dipping southwest between 40° and 60°. Where Mn oxides are absent, the veins are usually comprised totally of the hematite + magnetite and hydrated Fe oxide. The thickness is variable and can reach up to 4.0 m locally. Pyrolusite and psilomelane are seen in all of the samples (>about 15.0 modal %). This type of mineralization ore constitutes up to 60 wt % of the veins. The ore bodies are relatively zoned, with barite and manganocalcite forming the outer portions, and hematite, pyrolusite and quartz forming the cores of the veins. This type of vein contains 205,000 t of pyrolusite + psilomelane (proven reserves) with estimated ore reserves of over 1.0 Mt.

The pyrolusite + psilomelane + poliannite paragenesis occurs as thin lenses along strikes in the pyrolusite + psilomelane + hematite + barite ore and is observed mostly in the northwestern part of the area. Pyrolusite is the most common oxide mineral, ranging in amounts from 16 to 22 wt %. In addition to the major constituents of the ore, manganite, braunite and hematite in minor amounts are also present in this type of ore.

The barite + pyrolusite + psilomelane + hematite paragenesis forms lenticular orebodies trending mostly north-south, less northwest-southeast and dipping 50°–60° west and southwest, with a vertical extension of about 25 m. It is essentially in the form of a massive orebody where Mn-Fe minerals are absent. The thickness is variable and locally can reach up to 10 m. The ore-host rock boundary is considerably sharp. The relatively simple mineral assemblage of the massive barite ore includes barite (22.3–73.0 modal %), pyrolusite + psilomelane (2.3–18.7 modal %), hematite (1.6–7.9 modal %), calcite, quartz, and minor amounts of galena and pyrite. The ore contains 110,000 t of proven barite reserve, and locally grades into disseminated Fe-Mn oxide ores.

The Tumanpinari Fe-Mn-Ba veins show evidence of at least two periods of hypogene mineralization, separated by a period of fracturing and at least two periods of brecciation and cementations (Figure 4). The early regional fault systems caused the extensive fracturing, probably during emplacement of the volcanic rocks (phase A, Figure 4). Large amounts of hematite, pyrolusite and psilomelane were precipitated from phase A fluid in fault zones. The main mineralization stage is mainly associated with these fluids, and minor amounts of magnetite, barite, manganite, galena, braunite, poliannite and bixbyite were also deposited at this stage. Pyrolusite + psilomelane + hematite + barite ore and pyrolusite + psilomelane + poliannite ore are associated with this phase A. The fluids of phase A are partly responsible for the silicification, sericitization, hematitisation, and argillitic alteration of the host rocks. The phase A material was brecciated by renewed movements on the regional fractures, which permitted the introduction of a second Phase B mineralization. This is apparent from the fracturing, bending and microfaulting of the early-formed minerals. Compared with Phase A, Phase B

introduced less Fe-Mn oxide, and much more barite resulted from dilution of pyrolusite and hematite grade. The barite + pyrolusite + psilomelane + hematite ore (barite dominant ore) mainly was formed by the fluids of Phase B.

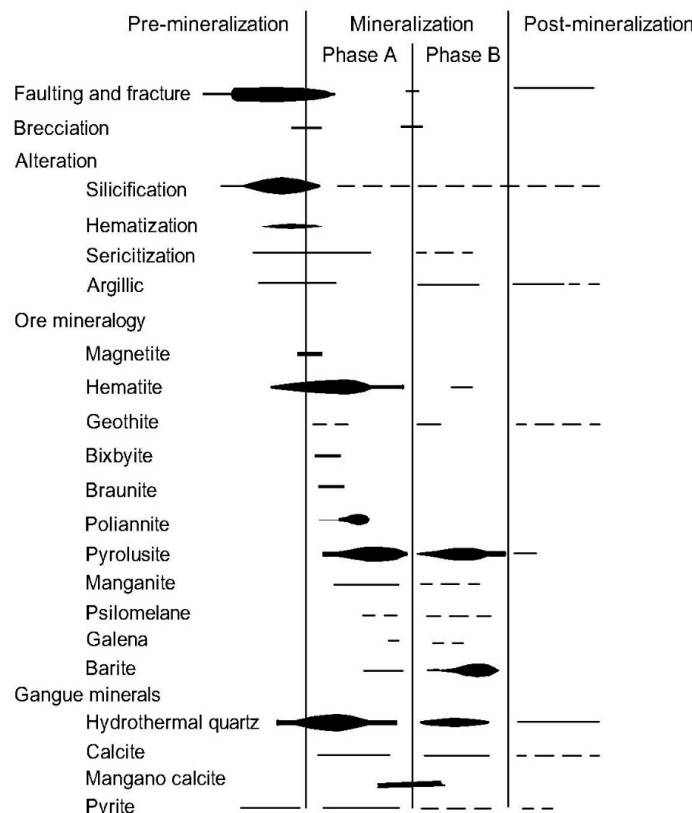


Figure 4. Simplified paragenetic sequence of events in the Tumanpinari area.

4.3. Geochemistry

Major and trace element data for a representative sample set of fresh and altered rocks and different ore types are presented in Tables 2 and 3. The volcanic rocks are mainly andesitic in composition, as is evident from the Zr/TiO₂ vs. Nb/Y ratio diagram [25], (Figure 5a). The range of andesite composition spans the medium-K to high-K fields on the classification diagram of Le Maitre (1989) [26]. (Figure 5b). Their total alkali contents range from 5% to 7%.

Table 2. Major and trace element contents of unaltered andesites. Major oxides in wt % and trace- and rare-earth elements in ppm.

Content	1	2	3	4	5	6	7	8	9	10
SiO ₂	62.85	62.41	62.96	59.95	63.10	60.36	61.91	58.91	62.36	59.37
TiO ₂	0.60	0.74	0.85	0.62	0.65	0.84	0.70	0.63	0.49	0.73
Al ₂ O ₃	13.61	16.63	15.92	18.13	17.18	16.52	16.09	14.87	17.51	15.69
Fe ₂ O ₃	6.81	5.88	7.98	4.53	5.12	6.21	5.98	6.84	5.20	5.96
MnO	0.08	0.13	0.15	0.05	0.03	0.96	0.20	0.11	0.13	0.10
MgO	1.39	1.53	0.79	1.29	1.69	1.74	0.98	3.57	1.46	1.80
CaO	5.60	3.80	2.91	6.70	2.90	4.71	7.04	5.93	3.98	5.52
Na ₂ O	3.03	5.07	3.17	2.23	4.45	2.62	2.48	3.18	2.44	2.34
K ₂ O	3.06	1.97	2.82	3.52	2.60	3.51	3.10	2.66	3.37	4.83
P ₂ O ₅	0.13	0.05	0.10	0.12	0.16	0.36	0.14	0.42	0.20	0.26
BaO	0.21	0.17	0.28	0.16	0.15	0.48	0.17	0.18	0.15	0.55
LOI	1.43	1.25	1.96	2.19	2.04	2.60	0.90	2.09	2.37	2.75

Table 2. Cont.

Content	1	2	3	4	5	6	7	8	9	10
Total	98.80	99.63	99.89	99.49	100.07	100.91	99.69	99.39	99.66	99.90
As	5.0	8.0	11	4.0	6.0	5.0	4.0	8.0	5.0	5.0
Cr	39	18	28	18	32	10	17	36	28	21
Co	20	13	21	13	22	16	6	16	12	14
Ni	40	49	43	38	50	37	33	48	39	42
Rb	230	190	170	190	280	170	200	200	250	200
Sr	560	550	620	550	320	610	450	550	480	650
Sc	18	14	12	14	12	13	10	14	13	17
V	110	190	150	190	114	94	68	180	70	94
Y	26	25	20	25	22	23	26	29	30	22
Zn	270	98	850	80	460	410	180	370	500	640
Zr	140	130	150	130	130	150	170	110	100	150
Nb	8.0	10	8.0	10	10	9.0	11	9.0	13	9.0
Cs	18	23	9.0	23	18	19	21	12	26	19
La	57	50	35	50	50	60	29	58	49	50
Ce	110	80	79	80	79	94	40	72	105	61
Sm	6.0	5.0	7.0	5.0	4.0	3.0	n.d.	4.0	6.0	5.0
Eu	1.0	1.0	1.0	1.0	0.5	0.8	n.d.	1.2	1.4	1.3
Yb	3.0	2.0	3.0	2.0	0.7	1.4	n.d.	2.4	2.7	2.1
Lu	0.4	0.3	0.4	0.3	0.1	0.1	n.d.	0.3	0.4	0.3
Hf	7.0	5.0	4.0	5.0	5.0	4.0	7.0	6.0	7.0	6.0
Ta	0.2	1.0	1.2	1.0	1.0	1.0	1.8	0.9	0.7	1.0
Pb	395	120	900	120	696	500	294	420	390	740
Th	30	24	20	24	26	23	22	24	30	21
U	7.0	6.0	4.0	6.0	5.0	6.0	4.0	5.9	4.5	6.3

n.d.: Not determined.

Table 3. Chemical composition of altered andesite and ore veins at Tumanpinari (Major element in %, trace- and rare-earth elements in ppm).

Content	1 (n = 4)	2 (n = 3)	3 (n = 3)	4 (n = 4)	5	6	7	8	9	10
SiO ₂	60.26	59.50	65.98	30.58	17.79	49.54	56.74	43.63	35.25	34.85
TiO ₂	0.74	0.68	0.51	0.34	0.33	0.20	0.01	0.05	0.05	0.07
Al ₂ O ₃	16.24	17.96	12.93	2.87	5.56	1.79	0.12	0.17	0.31	0.10
Fe ₂ O ₃	7.21	3.52	4.97	33.63	32.70	10.88	23.30	0.82	0.16	14.92
MnO	0.96	1.28	2.84	18.81	30.79	24.46	4.73	0.25	0.13	2.35
MgO	1.74	2.24	0.89	0.01	0.01	0.01	0.10	0.01	0.10	0.08
CaO	4.51	5.28	3.78	1.77	2.30	0.75	2.24	0.77	0.27	0.10
Na ₂ O	2.52	2.71	1.84	0.10	0.12	0.20	0.02	0.02	0.02	0.02
K ₂ O	2.41	3.01	2.78	-	-	0.03	-	-	-	-
P ₂ O ₅	0.36	0.31	0.44	0.05	0.05	0.10	0.01	0.01	0.01	0.01
SO ₃	-	-	-	2.86	5.51	3.13	3.21	17.83	22.35	17.25
BaO	0.48	0.47	2.03	6.35	3.80	5.85	9.13	36.17	40.93	30.18
LOI	2.57	3.04	0.91	2.64	1.05	3.10	0.42	0.30	0.45	0.10
As	8	10	25	1610	950	980	18	77	70	50
Co	22	20	6	18	6	10	<5	<5	<5	<5
Cr	32	13	7	14	15	4	3	2	3	3
Cu	46	26	12	140	100	87	160	97	120	80
Ni	50	55	23	56	10	110	40	30	18	16
Rb	475	290	200	15	5	22	40	10	30	20
Sr	325	270	150	530	560	600	9000	5400	11,000	5700
W	3	11	5	58	50	92	3	49	3	3
V	89	150	70	92	110	192	125	160	96	132
Y	10	5	6	4	4	4	n.d.	n.d.	n.d.	n.d.
Zn	200	140	7	1260	1050	1900	40	37	20	20

Table 3. Cont.

Content	1 (n = 4)	2 (n = 3)	3 (n = 3)	4 (n = 4)	5	6	7	8	9	10
Nb	10	9	6	8	11	10	5	5	5	5
Cs	12	9	14	10	14	16	9	10	9	9
La	50	24	29	4	5	6	4	5	5	2
Ce	79	54	40	3	3	3	<3	<3	<3	<3
Sm	3.1	2.9	3.8	0.2	0.2	0.1	0.1	0.1	0.2	0.1
Eu	1.6	0.9	1.0	1.7	2.4	1.6	0.3	0.3	0.2	0.2
Yb	2.3	1.9	0.7	0.2	0.2	0.1	0.5	0.3	0.3	0.5
Lu	0.3	0.1	0.1	0.1	0.1	0.03	0.03	0.03	0.03	0.03
Hf	5	6	5	4	5	n.d.	n.d.	n.d.	n.d.	n.d.
Ta	1	1	1.2	0.8	0.6	0.2	0.3	0.2	0.4	0.2
Pb	690	310	290	1000	3400	930	7800	12,000	900	3200
Th	0.8	0.5	0.2	0.3	0.5	0.5	0.2	0.2	<0.2	<0.2
U	3	5	4	6	5.0	5.5	7.0	4.0	7.0	6.0

n.d. = not determined; samples 1 to 3 are altered andesite; 1: moderately hematized; 2: argilic alteration; 3: silicified; 4: Pyrolusite + psilomelane + hematite + barite ore; 5,6: pyrolusite + psilomelane + polianite ore; 7 to 10: Barite-dominant ore.

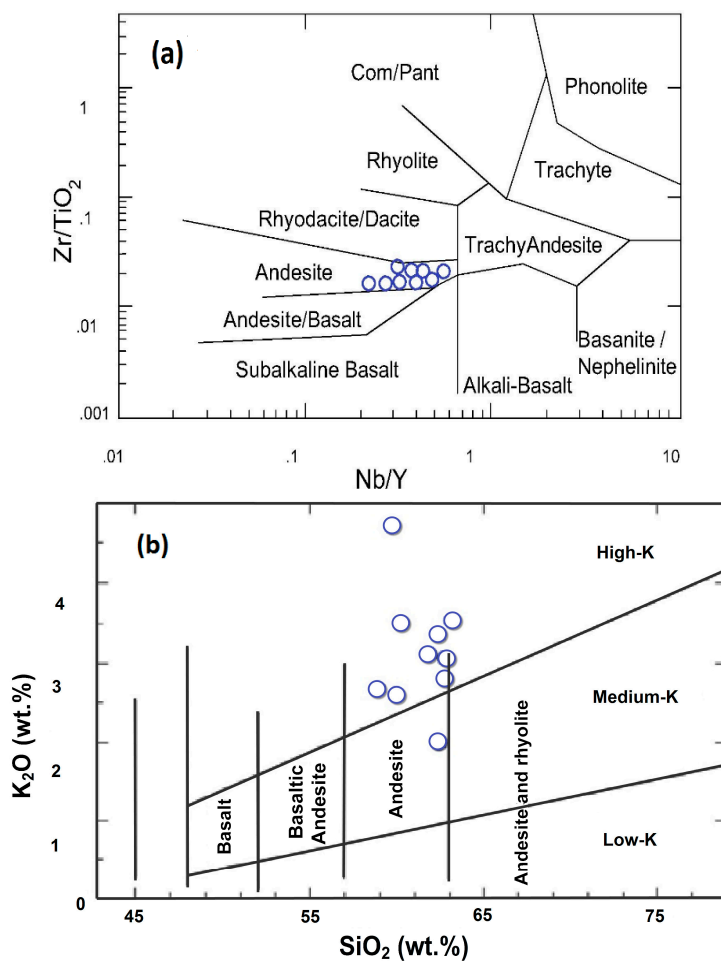


Figure 5. (a) Plot of volcanic rocks on Zr/TiO₂–Nb/Y ratio diagram [26]; (b) Position of samples on K₂O–SiO₂ variation diagram [7].

These rocks are moderate to strongly enriched in highly incompatible elements such as K, whereas they are depleted in compatible elements such as Mg, Ni, and Cr. On the primitive mantle-normalized diagram, andesites are enriched in LIL (Large ion lithophile) elements with respect to LRE (light rare

earth) elements and HFS (high field strength) elements and depleted in HFS elements with respect to neighboring LIL and LRE elements (Figure 6).

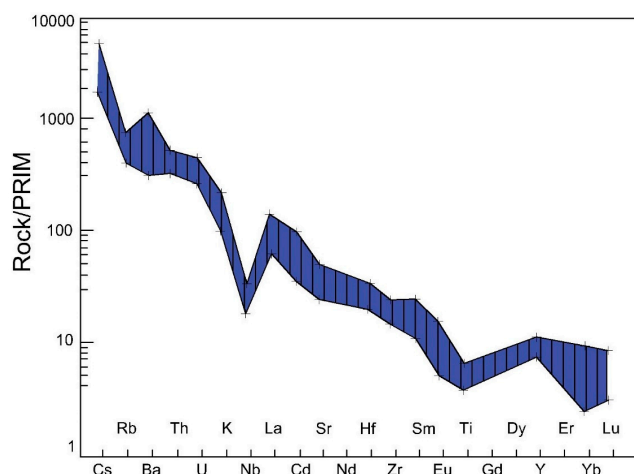


Figure 6. Trace element concentrations normalized to the composition of primitive mantle.

The average content of LIL elements such as Rb (210 ppm), Ba (3100 ppm), Sr (530 ppm) are also high, and there is a positive linear correlation ($r = 0.70$) between LIL enrichment and alkalinity. The low ratio of K/Rb is similar to values derived from the continental crust. Another significant characteristic of these rocks is the enrichment in rare earth elements (REE). Absolute LRE abundance is higher than that of average calc-alkaline rocks but closer to the values shown by high-K calc-alkaline andesite [7]. TiO₂ contents range from 0.5% to 0.9%. High field strength elements such as Zr, Nb, and Ta have an average of 140, 10 and 1.0 ppm, respectively, showing low to moderate concentrations.

In general, the trace element geochemistry of the Tumanpinari andesites shows typical characteristics of the andesite from the western Anatolian rhyolite-dacite-andesite-trachyte-basalt sequence [1].

The Tumanpinari ore bodies are strongly enriched in certain metals. In addition to the economically important elements of ore (i.e., Fe, Mn, Ba), most samples indicate substantial quantities of Pb, Zn, As and Sr. As indicated by chemical analysis, an increase in Pb and Sr and a decrease in As and Zn was determined along the axis of the veins towards the south. This elemental zoning is different from the hydrothermal alteration zoning developed in the volcanic rocks. The distribution of selected major and trace elements in the hanging wall and footwall of both barite-dominant ore and Fe-Mn oxide ore was studied on several profiles, two of which are shown in Figure 7. According to these profiles, the contents of trace element increase not only in the orebodies but also in the hanging wall rocks. The distribution pattern for As and Zn are considerably different for two ore types. The former element reflects a stronger peak in the Fe-Mn oxide orebody, while the latter does not show any meaningful change in the massive barite ore body. The rapid decreases of Fe, Mn, Ba, Pb and As to the regional background contents outside the orebodies reflect the sharp boundary of ore-host rock as well as the similar mobility of these elements in the volcanic rocks. Consistent with the similar ores of western Anatolia, manganese is generally at the level of the regional background of wall-rocks [9,10,27,28].

The chemical analysis results of altered andesitic rocks are given Table 3. Similar to the ore veins, the altered andesitic rocks are also enriched in certain elements (Si, Ba, Sr, Pb, Zn). In addition to the chemical similarity, some samples from the altered rocks contain the disseminated ore minerals such as pyrolusite, hematite and barite, as well.

The chemical results indicate that the transition from fresh to altered rocks has little effect on the elemental levels of Si, Al, Fe, Ca, Mg, K, Rb, Sr and H₂O⁺. The feldspar destruction and probably formation of secondary mica during alteration caused a change in Rb, Sr, and H₂O⁺ contents.

According to the plot of Sr vs. Rb, there is a negative correlation among pairs of elements (Figure 8a). The plots of H_2O^+ vs. Sr and H_2O^+ vs. Rb show a moderate decrease of Sr, and a marked increase in Rb and H_2O^+ contents (Figure 8b,c). However, the variation in MgO is consistent with the preferential formation of an Mg-bearing mineral within plagioclase such as smectite. The extreme increase of structural H₂O during alteration is mainly related to the argillic alteration. The decrease of Sr also reflects the replacement of the abundant plagioclase in the unaltered rocks and the importance of this mineral as a host for Sr. A plot MgO vs. H_2O^+ shows a marked increase of MgO and is consistent with the formation of clay minerals evolved during the processes of argillic alteration (Figure 8d). Figure 8e shows that hydrothermal fluids are enriched in P and Si.

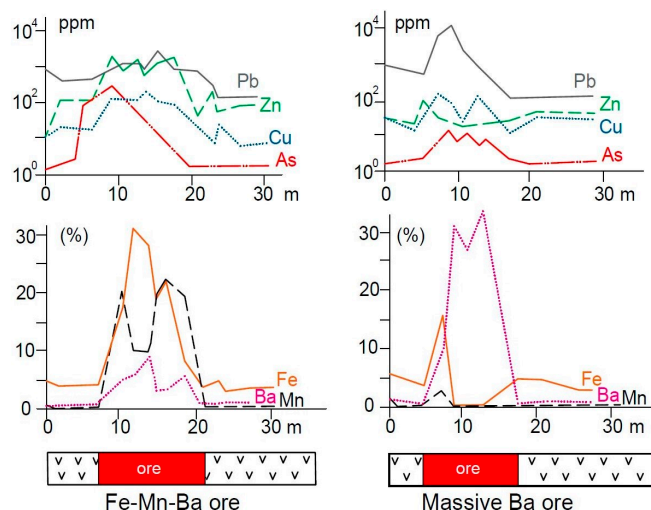


Figure 7. Variation in the concentrations of some elements in two sections crossing the Fe-Mn-Ba and Ba ores at Tumanpinari.

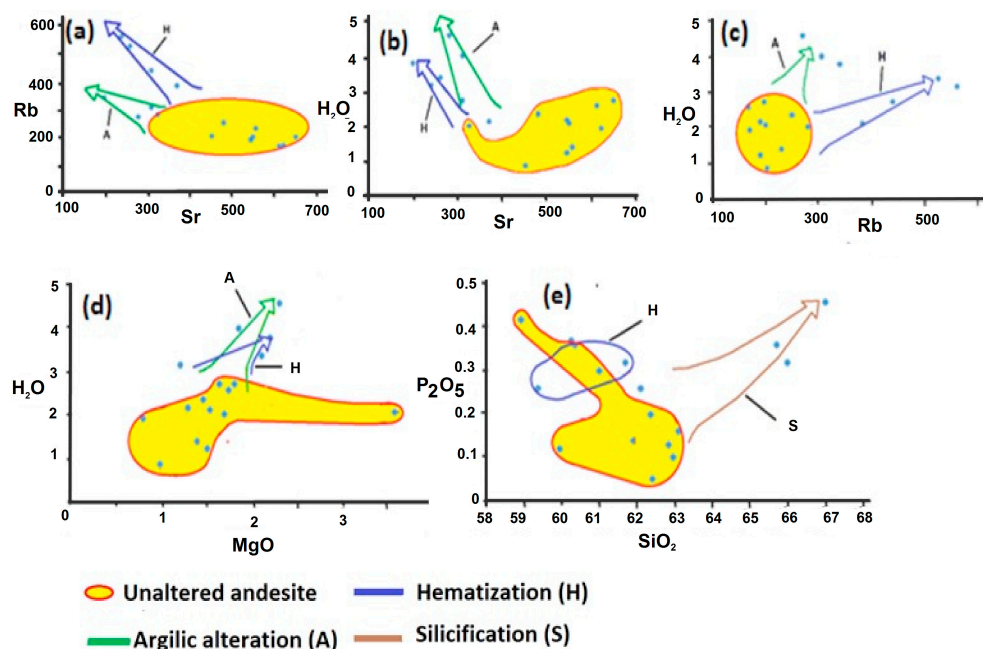


Figure 8. Binary plots of (a) Rb vs. Sr; (b) H_2O vs. Sr; (c) H_2O vs. Rb; (d) H_2O vs. MgO ; and (e) P_2O_5 vs. SiO_2 for the unaltered and altered andesite.

Geochemical characterization of the ore types is shown in Table 3. Analytical results for the Fe-Mn ore are given in two categories as mentioned earlier: pyrolusite + psilomelane + poliannite ore, and pyrolusite + psilomelane + hematite + barite ore. The Tumanpinari Fe-Mn ore is characterized by low Fe/Mn ratios, ranging 0.4 to 2.3. In addition, the high abundances of some trace elements such as As, Pb, and Zn seem to be one of the most important chemical features of the Tumanpinari deposit. However, there is some differences among the ore types, with respect to the distribution pattern of these elements. A major difference is that the barite ore contains high Pb and Sr whereas the Fe-Mn ore contains the high As and Zn values. In general, the abundances of minor and trace elements are suitable with characteristics of hydrothermal deposits associated with the volcanic activity. The As content is considered to be a significant geochemical criteria to identify the hydrothermal origin of the Tumanpinari deposit. The average content of this element in the barite and Fe-Mn ore is 54 ppm and 1270 ppm. The relationship between the Pb and Zn distribution indicated that the deposits have been affected more and less by supergene processes. A negative correlation has been observed between these two minerals

4.4. Fluid Inclusion

4.4.1. Petrography

On the basis of optical observations and microthermometry, two main types of fluid inclusion (Type I and II) were recognized. Each group was characterized by a specific shape, degree of fill (ratio of liquid to total volume of fill at 25 °C), salinity and homogenization temperature (Table 4, Figure 9).

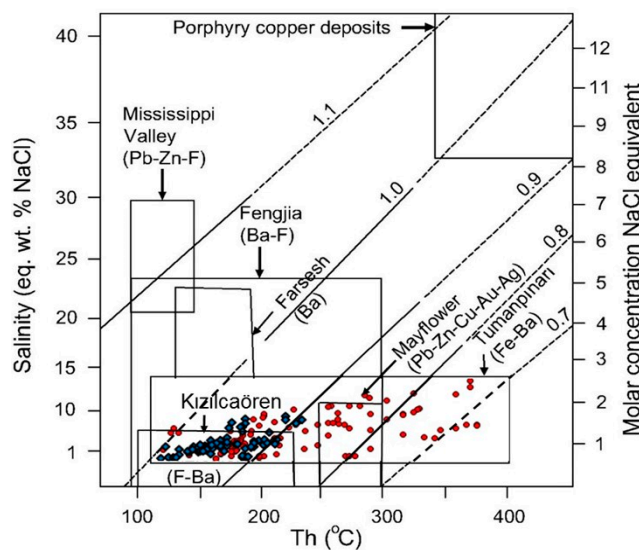


Figure 9. Homogenization temperature (Th) versus salinity for primary fluid inclusions contained in quartz and barite. Diagonal grid lines show fluid densities in gm/cm^3 from the system $\text{NaCl}-\text{H}_2\text{O}$ [29]. Data from porphyry copper deposits, Mississippi Valey, Fengjia, Farsash, Mayflower and Kızılıcaören are from [30–35]. The inclusions in Tumanpinari quartz and barite is shared by data from Fengjina, Farsash and Kızılıcaören deposits containing Ba and F. (red point: quartz; blue point: barite).

Table 4. Fluid inclusion data from Tumanpınarı Fe-Mn-Ba deposits.

Sample	Mineral	Fluid Inclusion Data	Volume of Fill	Number of Fluid Inclusion	Th (°C)	Salinity (eq. wt % NaCl)	Homogenization to Vapor (V) Liquid (L)	Type of Inclusion	Remarks
Kuzey damarlara area									
KD-6	Quartz	P	0.45	6	195–304	0.6–12.2	V	T1	V
KD-11	Quartz	P(S)	0.65	12	183–210	1.8–8.4	L	T1	V
KD-12	Barite	S	0.90	8	165–190	0.4–4.9	L	T2	B
KD-16	Quartz	P	0.50	8	273–403	10.3–14.9	V	T1	V
KD-17	Quartz	P	0.60	4	179–279	1.0–8.9	L	T1	B
KD-23	Barite	P	0.95	13	169–188	1.3–3.9	L	T2 (T1)	V
KD-23	Quartz	P	0.35	5	224–238	2.9–9.5	L	T1	V
KD-25	Quartz	S(P)	0.60	2	140–178	1.1–5.6	L	T2 (T1)	V
KD-25	Quartz	P(S)	0.35	11	205–356	0.6–9.7	L	T1	B
KD-26	Quartz	P	0.35	12	286–410	0.9–6.8	L	T1	B
KD-30	Barite	P	0.95	2	115–169	2.1–3.9	L	T2	V
KD-30	Quartz	P	0.75	2	222–249	1.2–5.5	L	T2	V
KD-33	Quartz	P	0.80	8	123–309	5.3–11.8	L	T2	V
KD-34	Quartz	P	0.50	4	210–354	3.8–9.5	L	T1	V
Güney Damarları area									
GD-2	Barite	P(S)	0.85	5	140–175	1.7–4.3	L	T2	V
GD-5	Barite	P(S)	0.92	9	138–169	1.6–3.9	L	T2	V
GD-6	Quartz	P	0.45	5	190–230	0.7–8.3	L	T1	V
GD-6	Barite	P	0.80	12	160–192	1.3–7.8	L	T2	V
GD-13	Barite	P	0.95	4	120–183	0.6–3.1	L	T2	V
GD-14	Barite	S	0.96	4	113–175	0.5–2.9	L	T2	V
GD-20	Quartz	P	0.70	6	198–245	2.5–7.6	L	T1 (T2)	B
GD-20	Barite	P	0.65	10	192–222	0.8–4.0	L	T1 (T2)	V
GD-21	Barite	P	0.90	7	122–185	0.4–3.2	L	T2	V
GD-25	Barite	P	0.87	12	148–169	1.7–3.8	L	T2	V

eq.: Equivalent; V: Vein filling ore; B: Breccia ore; T1, T2: Type I and type II inclusion; P: Primary; S: Secondary.

At room temperature, Type I inclusions were observed in quartz occurring in a matrix of vuggy silica and breccia. These types of inclusions are mainly two-phase, liquid-vapor inclusions, occurring either as single inclusions, or as clusters and planes of inclusions in the pyrolusite-dominant veins. This type of inclusions is considered primarily because they are confined within specific growth zones of the host minerals [22]. In some case, the inclusions appear to contain one phase (vapor) at room temperature, although many contain a considerable amount of liquid. The degree of fill ranges from 0.35 to 0.60. This type of inclusions shows consistent liquid-vapor ratios. The majority of the inclusions have negative crystal, elliptical and irregular shapes and are usually small (1–30 μm in size) with liquid-vapor ratios of 2.0–5.7. Typically, inclusions <1 μm in diameter are not suitable for microthermometric measurements. Type I inclusions also reflect secondary morphologies in quartz inclusions (Table 4).

Type II inclusions occur in barite crystals and show sub-negative crystals that are relatively regular in shape, with spherical or elliptical vapor bubbles. This type of inclusions must be younger than Type I inclusions and vary in size (5–65 mm). They are two-phase (L+V), very liquid rich or monophase liquid inclusions. Type II inclusions occur mostly as isolated primary inclusions, but in some cases also occur as secondary inclusions. These inclusions crosscut numerous inclusion-rich planes and are distinguished by the presence of several secondary morphologies. The degree of fill ranges from 0.65 to 0.96.

4.4.2. Microthermometric Results

Heating measurements for Type I inclusions obtained from quartz yield final homogenization temperatures ranging from 179 to 410 °C, with a few measurements above 400 °C (Figure 9). Primary Type I inclusions display first ice melting between –17.1 and –13.2 °C suggesting a solute composition dominated by NaCl + MgCl and a last ice melting temperature between –8.9 and –0.4 °C indicates maximum salinities of 14.9–0.6 eq. wt % NaCl.

Type II inclusions from barite have final homogenizations between 113 and 222 °C, but the majority of the measurements are between 148 and 222 °C. The lowest salinity values were measured in inclusions in barite. They are mostly primary inclusions and showed no evidence of gas upon cooling and no decrepitation occurred prior to homogenization. In all of the inclusions in barite, the vapor bubble progressively decreased in volume during heating prior to decrepitating, implying that they would have homogenized to the liquid (Table 4). First ice melting for Type II in barite occurred ≥ -24 °C, suggesting a solute composition of NaCl ± KCl. Final ice melting occurred between –4.8 and –0.2, indicating the salinity values between 7.8 and 0.4 eq. wt % NaCl. Some secondary Type II inclusions show metastable ice in the absence of a vapor phase during cooling. Therefore, the results for cooling were obtained from the inclusions that showed stable ice melting in the presence of a vapor bubble.

4.5. Sulphur Isotopic Composition

Sulphur isotopic results are listed in Table 5. The $\delta^{34}\text{S}$ values of the Tumanpinarı samples (barite, $n = 9$; pyrite, $n = 4$) show completely positive values, ranging from 3.12‰ to 6.21‰. Barite in the barite-dominant ore ($n = 7$) and in the Pyrolusite + psilomelane + hematite + barite ore ($n = 2$) has similar $\delta^{34}\text{S}$ values, ranging from 3.23‰ to 6.13‰. The average $\delta^{34}\text{S}$ value of barite for the two types of ores are 4.62‰ and 4.20‰, respectively. The $\delta^{34}\text{S}$ values of pyrite samples were also similar like the barite samples, and reflect the S isotopic composition of disseminated pyrite with an average $\delta^{34}\text{S}$ value of 4.56‰ and are completely associated with the pyrolusite + psilomelane + hematite + barite ore.

Table 5. Sulphur isotopic data on Tumanpinari deposits.

Sample	Minerals	Ore Type	$\delta^{34}\text{S} \text{\%}$ V-CDT	Sample	Mineral	Ore Type	$\delta^{34}\text{S} \text{\%}$ V-CDT
GD-2	Barite	Barite-dominant ore	4.2	KD-12	Barite	Pyrolusite + psilomelane + hematite + barite ore	3.6
GD-5	Barite	Barite-dominant ore	5.6	KD-18	Barite	Pyrolusite + psilomelane + hematite + barite ore	4.8
GD-18	Barite	Barite-dominant ore	3.3	KD-22	Pyrone	Pyrolusite + psilomelane + hematite + barite ore	3.6
GD-20	Barite	Barite-dominant ore	4.9	KD-26	Pyrone	Pyrolusite + psilomelane + hematite + barite ore	6.2
GD-21	Barite	Barite-dominant ore	3.2	KD-28	Pyrone	Pyrolusite + psilomelane + hematite + barite ore	3.1
GD-22	Barite	Barite-dominant ore	5.1	KD-30	Pyrone	Pyrolusite + psilomelane + hematite + barite ore	4.2
GD-25	Barite	Barite-dominant ore	6.1				

5. Discussion

5.1. Characterization of Hydrothermal Fluids

The microthermometry studies provide significant data revealing formation conditions of the Tumanpinarı deposit. In order to easily understand the characteristics of hydrothermal fluids at Tumanpinarı, the results have been compared with a few selected epigenetic deposits containing fluorite, barite and some metallic minerals [21,30–36]. Homogenization temperatures versus salinity for primary fluid inclusions in quartz and barite are plotted in Figure 9. In the figure, the high-salinity and high-temperature values of the inclusions belonging to the porphyry copper deposits are plotted in the upper right corner of diagram. This type of deposits point to either a fluid of probable magmatic origin circulated in the porphyry system or the mixing of magmatic and meteoric fluids [1,37,38]. In general, the relatively high-salinity (about 20 eq. wt % NaCl), low-temperature 150–275 °C inclusions may have been the result of episodic mixing of deep-saline brines of probable magmatic derivation with low-salinity meteoric fluids [25,38,39]. In Figure 9, these are represented by the samples from Farsesh Ba deposits, Kızılcaören barite-bearing fluorite deposits, and relatively Fengjia barite-fluorite deposits. The Tumanpinarı barite and quartz samples mostly yield microthermometry data similar to epithermal fluorite-barite mineralization at Kızılcaören, and partly the barite-fluorite mineralization at Fengjia. The Tumanpinarı hydrothermal system reflects a change from the high temperature-salinity stage towards low temperature-salinity stage. It is clear that the value of high-salinity is related with the magmatic fluids, but they could also have been generated by heated basinal brines. Therefore, the relatively high-salinity and low-temperature inclusions can be good evidence for mixing between magmatic and meteoric fluids in the Tumanpinarı epithermal system.

The fluids related to Fe-Mn ores at Tumanpinarı are probably represented by Type I inclusions. This fluid is also partly responsible for hydrothermal alteration. The fluid inclusion Types I (Quartz) and II (Barite) identified at Tumanpinarı have different homogenization temperature and salinity ranges (Figure 10). The fluid inclusions in quartz and barite have an average temperature of 279 °C (range 123–410 °C) and 153 °C (range 113–192 °C), respectively. The presence of some liquid-rich and vapour-rich inclusions from the same generation of fluid is interpreted as evidence of boiling [22]. This feature is commonly observed in many volcanic rocks-hosted hydrothermal Pb-Zn and Fe-Mn deposits in western Turkey [1,11,40]. At Tumanpinarı, some Type I inclusions have high homogenization temperatures, low salinity values, and highly variable vapor/liquid ratio. The relationships between homogenization temperature and low-salinity of Type I inclusion is not straightforward, probably reflecting that these inclusions were trapped under boiling conditions. Specifically, in a single sample, an inverse relationship between homogenization temperature and salinity is consistent with a boiling fluid process and stream loss (Figure 10).

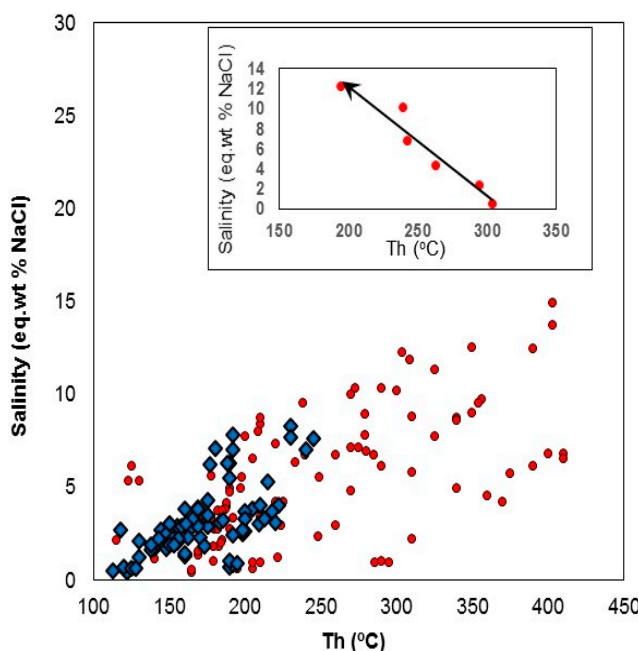


Figure 10. Salinity vs. homogenization temperature (Th) plot of fluid inclusions from quartz and barite. Internal plot shows trend of increasing salinity with decreasing temperature in sample KB-6. This observed trend is associated with a positive increase of salinity due to streamloss under boiling conditions (red point: quartz; blue point: barite).

The high homogenization temperatures measured in Type I inclusions from quartz indicated that the quartz is probably of magmatic-type. Compared to the temperature ranges proposed by Lindgren (1933) [41] for epithermal deposits, the temperature range measured for the deposit is relatively high. In general, the temperature ranges formed at shallow levels (<1 km depth) within crust can form over a wide temperature range (100–400 °C) [34]. Moreover, the high temperature range can also be associated with different fluid generations or heterogeneous trapping and/or necking down phenomena [29,31].

Type II inclusions with lower salinity (0.4–5.6 eq. wt %) and temperatures (113–222 °C) record the late-stage hydrothermal fluids responsible for barite mineralization. This fluid type is typical for many epithermal Ba deposits in western Anatolia [1,35]. Some of Type II inclusions in barite crystals were probably trapped close to boiling conditions, due to the absence of vapor-phase-bearing inclusions which point out a deficiency.

The fluids which cause the hydrothermal mineralization at Tumanpinarı were also responsible for ore-stage hydrothermal alterations. The amounts of alteration minerals are lower than those of early hydrothermal activity. The intimate textural relationship between euhedral hydrothermal quartz crystals and the pyrite lining vuggy silica fractures were observed. These textural relationships suggest that the inclusions in hydrothermal quartz probably contain the fluid present during the deposition of pyrite co-evolved with hydrothermal quartz crystals.

The hydrothermal alteration affected large areas of the andesitic host rock indicating that the mineralizing fluids are extremely hot. This is consistent with the temperature obtained from the fluid inclusion data (113–410 °C). At Tumanpinarı, hydrothermal activity caused the occurrence of some mineral assemblage in the wall-rock alteration zones (Table 1). Alteration mineral assemblages may give some information on temperatures during the evolution of the hydrothermal system. According to Sawkins, 1990 [34]; and Cooke et al. (1996) [42], chlorite and sericite (illite) form between 200 °C and 300 °C in geothermal systems. The main hydrothermal alteration assemblages at Tumanpinarı (sericite, chlorite, kaolinite and montmorillonite) are therefore interpreted to have formed at high temperatures (>200 °C), which is consistent with the fluid inclusions data.

In a microthermometry study, a pressure correction becomes necessary when the total pressure at the time of entrapment is greater than the vapor pressure of the fluid [38], so the pressure correction is the amount that must be added to the homogenization temperature of an inclusion to obtain the true trapping temperature. Temperatures of homogenization are reported uncorrected for pressure, and are presumably close to the formation temperature, because of the presence of fracture fillings at shallow depths.

5.2. Source of Sulfur and Metals

Geochemical data from the Tumanpinarı ore provide important information regarding the source of metals. The veins are rich in Mn, Fe, Ba, Pb, Zn, and As, and do not contain Ag and Au. Similarly, altered volcanic rocks are enriched in some elements such as Si, Ba, Pb, Zn, and partly in P₂O₅. This enrichment is undoubtedly related to the hydrothermal systems. At Tumanpinarı, major and trace element composition of the andesites showed high values of Ba, Pb, Zn and normal values of Fe, Mn. The average Fe, Mn, Ba, Pb and Zn contents of these rocks ($n = 10$) are 6.05%, 979 ppm, 3100 ppm, 458 ppm and 385 ppm, respectively. These geochemical results suggest that the source of metals for the ore veins is not only altered rocks but also a primary magma which is an important source, especially for Mn. In other words, a dual metal source such as magma and wall rocks for hydrothermal fluids is likely possible at Tumanpinarı deposits. The relative increase of P₂O₅ and the accompanying increase of SiO₂ in the silicified altered rocks are related to the P-and Si-rich hydrothermal fluids from which thin quartz veinlets containing apatite formed. In light of present data, however, it is difficult to conclude whether the elevated contents of elements in the veins represent a supergene enrichment or not.

Sulphur isotopic composition of barite and pyrite suggests a magmatic source or leaching of primary magmatic sulphides from volcanic rocks (Table 5). The indistinguishable sulphur isotope values of pyrite and barite from those of the surrounding volcanic and intrusive rocks further support the magmatic source. The range of $\delta^{34}\text{S}$ values from the samples ($n = 13$) markedly coincide with the range of magmatic values [43]. Generally, the narrow range of $\delta^{34}\text{S}$ values indicate that the hydrothermal fluids originated from the same sulphur source that its $\delta^{34}\text{S}$ composition was constant at the deposits' scale during the ore formation [43,44].

In geochemical studies, Co:Ni ratios in ore minerals are commonly used to differentiate between submarine exhalative, magmatic or sedimentary origin of ore deposits [34,44]. Some authors also reveal that Co:Ni ratios of pyrite in particular may be reliable indicators of ore genesis deposit [45,46]. Hydrothermal pyrite generally contains >400 ppm Co and a Co:Ni ratio >1, whereas sedimentary pyrite has >100 ppm Co and a Co:Ni ratio <1. This mineral in volcano-sedimentary deposits are characterized by Co:Ni ratios of >5 and commonly >10 [45,46]. Rao and Naqvi (1977) [44] reported that preferential concentration of Co in pyrite is related to the higher crystal field stabilization energy of Co²⁺, as well as to the compatible electronic spin states between Co²⁺ and Fe²⁺. According to the previous geochemical studies in the Tumanpinarı deposit [10], pyrite is characterized by high-Co values (329–715 ppm) and high-Co/Ni ratios (2.1–4.5). The Co:Ni ratios and Ni contents of the Tumanpinarı pyrite clearly indicate their derivation from magmatic sources. The analyzed pyrite samples have lower Co:Ni ratios than those associated with volcano-sedimentary and higher Co:Ni ratios than sedimentary pyrite.

5.3. Temperature–Depth Relationship

The values of homogenization temperature and salinity are used to estimate the depth of mineralization, using the temperature–depth diagram of Haas (1971), [47]. A similar approach was successfully applied to the Arapuçan and Kızılcaören epithermal deposits, and the results indicated great compatibility with the stratigraphic section [1,35]. In epithermal systems, hydrothermal activity is usually characterized by hydrostatic pressure. Considering this fact and the shallow level of emplacement, the pressure correction should be minimal, and the T_h of fluid inclusions probably close to actual trapping temperature. Fluid inclusion data, however, may give some information on pressure

conditions during the evolution of the Tumanpinari epithermal system. If it is assumed that the inclusions were trapped under boiling conditions, then the depth of trapping can be estimated using the boiling-point curves for H_2O liquid (0 wt percent) and for brine of constant composition given in wt % NaCl of Haas [29,47]. According to the author, it is possible to estimate the maximum depth below the water table at which a crystal grew if the inclusions in the crystal indicated there was boiling at the time of growth. The range and average T_h for the type I inclusions in hydrothermal quartz are shown in Figure 11, plotted against the depth. In the same figure, the boiling curves (from pure water to 25% NaCl) are also reported. T_h data of type I inclusions together with their average salinity values show that the depth at the time of epithermal mineralization could be between approximately 400 and 675 m below the paleo water table. This depth range corresponds to 32–55 bars under hydrostatic conditions [47,48]. The estimated depths are consistent with the field evidence of the Cenozoic section at Tumanpinari.

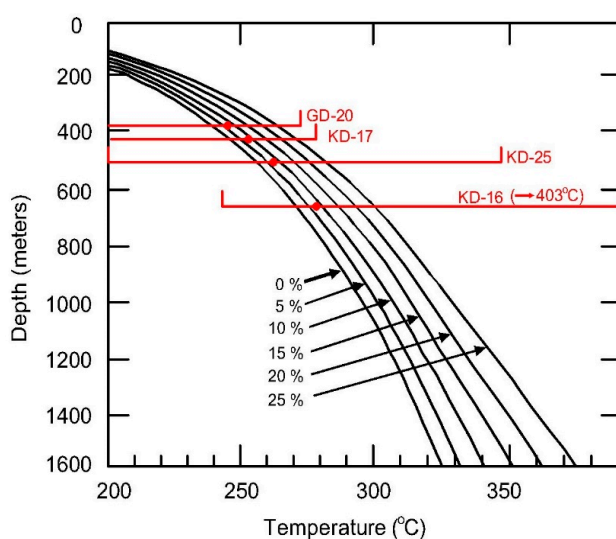


Figure 11. Temperature vs. depth diagram with boiling-point curves for H_2O liquid (0 wt %) and for brine of different compositions given in wt % NaCl. The temperature at 0 m of each curve is the boiling point for the liquid at 1.013 bars (1.0 atm) load pressure [47].

5.4. Ore Deposition

The Tumanpinari ore deposit occurs as veins in the fault zone of andesites outcropping in the Havran-Dursunbey district. The andesitic rocks hosting different vein types of ores are a product of calc-alkaline volcanic affinity and have been exposed to extensive hypogene alteration, partly at the time of their deposition and, later, at the time of mineralization. The textural and mineralogical features of the hydrothermally altered rocks provide a link between the alteration processes and mineralization. The hydrothermally altered rocks essentially result from the low temperature hydrothermal conditions. In the Havran-Dursunbey district, the fault systems, especially post-mineralization fault systems, generally define the geometry of the ore deposits. The Tumanpinari ore veins that cross-cut the alteration zone mostly occur as open-space drillings in less disseminated ore types. The massive character of the veins is a most common feature. On the other hand, the presence of feldspar with fine-grained sericite in the veins provides a good indication of ore-stage hydrothermal alteration. The length of the veins is similar to the other epigenetic Fe-Mn-Ba veins in the Havran-Dursunbey district and is rarely above 1 km. Their thickness is markedly increased at the intersections of the faults.

The hydrothermal fluids that caused alteration and mineralization probably followed similar paths. During the transporting of elements, the ore forming fluids were mixed with the meteoric fluids at the upper levels and caused a decrease of mineralization temperature (Figures 10 and 11).

The mineralogy of the Tumanpinari deposit is relatively simple, whereas it was complex in similar veins taken from the west of Havran-Tumanpinari district. The four minerals; pyrolusite, psilomelane, hematite and barite, constitute more than 90% of the total ore assemblage. Pyrolusite + psilomelane + hematite + barite paragenesis is a dominant ore and constitutes 60% of the total reserves. Barite-dominant ore is characteristic of the southern veins. The presence of galena, braunita and bixbyite, as well as high contents of As, Pb and Zn, in the Mn-Fe-Ba veins is a good indication of hydrothermal deposits. In general, the texture of the ore minerals is quite similar in all type of paragenesis. On the basis of minerals, pyrolusite is the most common ore mineral and found in all types of paragenesis.

The Tumanpinari Fe-Mn-Ba deposit occurs adjacents to each other in two different areas. The veins of both Kuzey Damarlar and South Damarlar area have broadly similar mineralogical, paragenetic, and geochemical relationships. Although differing in detail, the overall textural and paragenetic similarity of the major minerals, as well as the physical proximity of two areas of mineralization suggest that they are closely related, and probably formed during a single evolving period of deposition.

The Tumanpinari deposit is enriched in certain metals such as Pb, Zn, As and Sr, as well as economically important elements such as Fe, Mn and Ba. The Pb and Sr content is higher in the southern veins than that of northern veins. Contrarily, the As and Zn content is higher in the southern veins. In other words, the barite ore has high Pb and Sr content whereas the Fe-Mn ore has high As and Zn values. Similarly, the altered volcanic rocks are enriched in similar elements, such as Si, Ba, Pb, Zn, and partly in P_2O_5 . These data show that the ore veins and alterations of volcanic rocks develop from similar types of hydrothermal systems. The Tumanpinari Fe-Mn ore shows low Fe/Mn ratios, ranging 0.4 to 2.3, with a relatively low standard deviation.

The formation of Tumanpinari orebodies in the andesites has led to the need for more detailed examinations of these rocks. On the basis of petrographic and geochemical studies, the majority of Tumanpinari volcanic rocks show high-K calc-alkaline character and Rb and Sr contents and the initial Sr isotope ratio depends on the degree of fractionation [47]. On the primitive mantle-normalized spider diagram, andesites are enriched in large-ion lithophile elements (LIL) over high-field strength elements (HFS) and light rear earth elements (LRE), with the characteristics of orogenic magmatism [7]. Miocene calc-alkaline rocks including mostly andesite and, to a lesser extent, rhyodacite and dacite in the Dursunbey district have some geochemical characteristic data. The significant characteristics of this group are the lack of iron enrichment [7] and the titanium and barium contents of mica [49]. The rocks are hyperssthene and quartz-normative, total alkalis are high, ranging from 5% to 7%, LIL elements such as Rb (168–250), Ba (1300–4900), and Sr (325–650) are also high, and there is a positive correlation between LIL enrichment and alkalinity. The K/Rb ratio, averaging 250, is low and compares more favorably with values derived from the continental crust. The calc-alkaline suite of volcanic rock is also enriched in rare earth elements (REE). Absolute LREE abundances (100–200 times chondrite) are higher than those of average calc-alkaline rocks but closer to the values shown by high-K calc-alkaline andesites. TiO_2 content is generally low, usually less than 0.7%. High field strength (HFS) elements such as Zr (100–169), Nb (8–13), Ta (0.2–1.8) are also in low to moderate concentrations. The Sr^{87}/Sr^{86} ratios of these rocks range from 0.705 and 0.708 [7], occupying an intermediate position between mantle and continental crustal values. In addition, they have a significant feature in terms of mineral chemistry. Moderate- and high-Ti and Ba micas are found generally in alkaline magmatic rocks. However, at Tumanpinari, it is observed that low to moderate barium- and titanium-rich micas can be found associated with calc-alkaline magmatic rocks [49]. The most consistent feature of the micas is low to moderate Ba and Ti contents, up to 1.72 wt % BaO and 5.90 wt % TiO_2 , respectively. In conclusion, the geochemical and isotope evidence shows that calc-alkaline volcanic rocks are hybrids in term of crustal and mantle components.

5.5. Role of the Structural Factors and Age of Ore Deposition

Western Turkey, comprising the Havran-Dursunbey district, is characterized by a widespread post-Oligocene calc-alkaline volcanism. The calc-alkaline volcanic activity began during the Late Oligocene-Early Miocene in a compressional tectonic. This tectonic regime led to the general fracture systems that served as channels for rising calc-alkaline magma. The andesitic rocks related to the Tumanpinarı deposits were erupted in this period [7,16]. At Tumanpinarı, in addition to the porosity, permeability and most likely chemistry of the rocks, the regional tectonic played an important role in determining the nature of mineralization and the occurrence of fractures. On the basis of paragenesis and the field data, it is deduced that, at least, two separate sets of fractures (NW-SW and N-S) were moved repeatedly to permit the influx of mineralizing fluids. Pre-volcanic fracture systems controlled the structure and mineralization of veins, but major movements postdating the veins controlled their morphology and broke them up into blocks. The smaller and thinner orebodies are essentially associated with the radial faults suggesting that the radial fault systems were generated during the later phases of the main mineralization.

The Havran-Dursunbey district includes mostly the lens-shaped veins along the NW-SE- and N-S-trending faults of Late Oligocene-Early Miocene in age [7,10,12]. The veins and faults hosting the ore are markedly parallel to the regional faults. Overall, it can be easily said that the Tumanpinarı ore veins and their general morphologic occurrences and mineral assemblages were the result of structural factors, which also determined the location of the mineral. This evidence shows that the deposition probably occurred during eruption of the andesites or immediately after their replacement.

5.6. Ore Genesis Model

Numerous Miocene Mn oxide and Fe-Mn-Ba deposits were recorded in the Havran-Dursunbey metallogenic sub-province of western Turkey. The early studies conducted in the region revealed a marked relationship between Tertiary volcanism and Pb-Zn and, Mn-Fe-Ba ores [9,10,35]. The deposits mostly contain mineralization of vein type in the fault zone, and less metasomatic type in the tuffs. The Tumanpinarı Mn-Fe orebodies are completely in the andesites, whereas in the south of Balıkesir, around Bigadiç, some hydrothermal Fe-Mn-Ba veins were also found in the Tuffs. The deposition of the veins was controlled by both structure and lithology. The main veins, being mineralogically similar and coevolved together, occur in an area of approximately 4.0 km². The geological evidence indicates the close genetic association of faults with zones of hydrothermal alteration. According to field observation, the hydrothermal alteration zones formed roughly parallel to the ore veins.

Based on geochemical, mineralogical and isotopic data as well as field observations, a genesis model that covers all the systems was constructed and presented in Figure 12. The geochemical and isotopic characteristics of the andesite show that they are essentially associated with a mantle-derived magma generated in a subduction-enriched sub-continental lithospheric mantle, but the Tumanpinarı calc-alkaline volcanics crystallized from magma contaminated by crustal material, either in the source region or during ascent through the continent [7]. Pre-mineralization stage involves replacement of volcanic rocks and their alteration in which magmatic-derived gases were separated at depth from a hypersaline liquid. With little doubt, silicic cement of the breccia is essentially associated with this stage (Figure 12a). The early regional fault systems and extensive fracturing, probably during emplacement of the volcanic rocks, permitted the introduction of mineralizing fluids.

The second stage involves mixing of meteoric and magmatic-derived fluids. The magmatic-derived fluid, naturally hypersaline, rose at shallower levels and mixed with low-salinity fluids and this mixing was responsible for the precipitation of the ore. The hydrothermal system being responsible for transporting the elements created the conditions that favored the formation of the ore deposits. As a result of the leaching of element during the alteration of host rocks, the hydrothermal fluids became richer with respect to various elements such as Ba, Mn, Fe, Pb and Zn (Figure 12b). The last stage is presented by the formation of the many shallow-seated vein types of Mn-Fe oxides and barite (Figure 12c). Pyrolusite, hematite, and barite are the most common ore minerals occurring at this stage.

Magnetite, psilomelane, poliannite, pyrite and galena mostly accompanied these minerals. Sphalerite is not observed, despite the high Zn values in some samples. Fine-grained ore minerals in vuggy cavities, fractures in silica bodies, ore-veinlets cross-cutting the argillic zone, and fractures filled with ore minerals within the silicic breccia matrix show clearly that the ore formation stage postdated hydrothermal alteration. Precipitation of Ba-Mn-Fe, and gangue minerals took place under a large span of temperature conditions of hydrothermal systems which started at relatively high temperature conditions, near to the critical point of aqueous fluid systems, down to low temperatures.

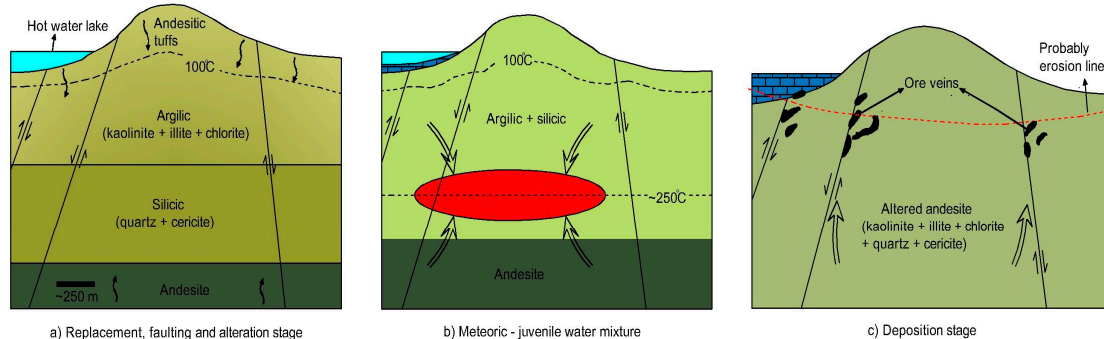


Figure 12. Ore genesis model for Tumanpinari.

At Tumanpinari, the post-mineralization stage is represented by the secondary Fe and Mn oxide deposition formed from removing Fe-Mn metals, and quartz and calcite veinlets. The veinlets cut all the formerly occurred mineral phases. Supergene enrichment products of Fe-Mn minerals seem to give a cut-to-ceiling view of the primary ore body in places.

Some lens-shaped stratified orebodies have been locally observed in pyroclastics rocks in the southern part of Dursunbey. There is overwhelming supportive evidence for epigenetic vein-type occurrences, but the depositional environment of stratiform type ore in tuffs, of course, raises the question of whether mineralization might have occurred under marine conditions. The presence of tuff might point in that direction, and the sulphur isotope ratio of the barite and pyrite samples taken from the stratified orebodies can be used to understand the precipitation of seawater sulphate. Generally, volcanogenic sulphate deposits are characterized by $\delta^{34}\text{S}$ values ranging from 0 to 8.5 with a mean of around 2‰ [29,50]. In western Turkey, the $\delta^{34}\text{S}$ values for epithermal type Mn-Ba deposits of Tertiary age range from 1‰ to 5.8‰ [47,51]. This overlap of $\delta^{34}\text{S}$ shows that sulphur isotope data from the Dursunbey stratified ore are compatible with the volcanogenic sulphate field, but cannot by themselves implicate a seawater origin. In western Turkey, tuffs were mainly deposited in small lacustrine basins and essentially hosted many borate and zeolite deposits. The relatively high-homogenization temperatures, low-salinity values, the sulphur isotopic results, the compatibility between the trace element geochemistry of volcanic rocks and the mineralization, the vein-type occurrences along faults, and confinement of mineralization to volcanic rocks indicate a similarity in the epigenetic Fe-Mn-Ba veins of western Turkey [49].

6. Conclusions

The Tumanpinari mineralization, mainly open space filling, is a product of hydrothermal systems and is genetically related to calc-alkaline volcanism of the Late Tertiary age. The deposit is prominently fault-controlled and, like the other Mn-Ba deposits of Havran-Dursunbey sub-province, at least some of the ores are in the fissure and breccia zones. Microthermometric measurements and the mineralogical and geochemical evidence with the presence of some short and irregular veinlets all indicate an epithermal deposition at Tumanpinari. All the orebodies have a relatively simple mineral assemblage. In general, the geochemical data on the Tumanpinari deposit are similar to that of volcanic-hosted Mn-Fe-Ba deposits of western Turkey. All these deposits are associated with post-Oligocene volcanic

activity. The source of metal is mainly magma, but some of the metal in the Tumanpinarı hydrothermal solution was derived from altered volcanic rocks. The solutions causing the mineralization show some differences in metal content. The Ba rich-fluid is enriched in Pb and Sr, whereas the Fe-Mn-rich fluid is enriched in As and Zn.

Two phases of mineralization have been defined in the deposit. The ore veins seem to have been deposited as a part of a large magmatic-meteoric water hydrothermal system. Fluid inclusion data indicate that the barite formed low-salinity (average 2.7 eq. wt % NaCl), low temperature (113–192 °C) fluids whereas, quartz from the pyrolusite + psilomelane + hematite + barite, and the pyrolusite + psilomelane + polianite ore was formed in slightly more saline (average 7.4 eq. wt % NaCl) and higher temperature (123–410 °C) fluids. The salinity measurements together with stable isotope data suggest the magmatic fluids rose at shallower levels and mixed with low-salinity fluids, i.e., with meteoric waters. During the late stages of mineralization, the system was predominantly diluted meteoric water. The microthermometric measurements show that the secondary type II inclusions are essentially aqueous and were obviously introduced after primary type I inclusions in the hydrothermal quartz showing undulose extinction

In the Tumanpinarı veins, mineral precipitation from hydrothermal fluids is from magnetite and hematite through Mn-oxides and barite, forming a marked characteristic of the veins. The geothermometric fluid inclusion studies show a formation environment of moderate temperature. The Fe-Mn minerals at Tumanpinarı are mainly deposited during the introduction of phase A liquid whereas barite occurrence is mostly related to phase B liquids. Geological evidence and the boiling-point curves associated with brine of constant composition show that the depth during the mineralization was approximately 400–675 m.

Author Contributions: Ali Haydar Gültekin wrote the paper, doing field and laboratory work as well as analyzed the data. Nurgül Balci contributed to the writing manuscript, analyzed the sulfur isotope data and contributed to the laboratory work.

Conflicts of Interest: The authors declare no conflict of interest.

References

1. Örgün, Y.; Gültekin, A.H.; Onal, A. Geology, mineralogy and fluid inclusion data from the Arapuçan Pb-Zn-Cu-Ag deposit, Çanakkale, Turkey. *J. Asian Earth Sci.* **2005**, *25*, 629–642. [[CrossRef](#)]
2. Bingöl, E. Contributions a L'étude Géologique de la Partie Centraleet Sud-East du Massif Kazdağ (Turquie). Ph.D. Thesis, Université de Nancy, Nancy, France, 1968. (In French)
3. Krushensky, R.D.; Akçay, Y.; Karaege, E. *Geology of an Area East of Edremit, Biga Peninsula, NW Turkey*; U.S. Geological Survey: Reston, VA, USA, 1971; p. 132.
4. Yücelay, M.A. Geological study of Karaköy-Arapuçan dere Pb-Zn-Cu mineralization, Çanakkale-Yenice. *Econ. Geol.* **1971**, *82*, 1575–1591.
5. Aydin, E.; Öztunalı, O. Occurrence conditions of the Pb-Zn mineralization of the Biga Peninsula. *Yerbilimleri* **1981**, *1*, 10–20.
6. Ağdemir, N.; Kırıkoğlu, M.S.; Lehmann, B.; Tietze, J. Petrology and alteration geochemistry of the Epithermal Balya Pb-Zn-Ag deposits NW Turkey. *Miner. Depos.* **1994**, *29*, 366–371. [[CrossRef](#)]
7. Yılmaz, Y. Comparison of young volcanic associations of western and eastern Anatolia formed under a compressional regime: A review. *J. Volcan. Geotherm. Res.* **1990**, *44*, 69–87. [[CrossRef](#)]
8. Ercan, T.; Satır, M.; Kreuzer, H.; Türkcan, A.; Günay, E.; Çevikbaş, A.; Ateş, M.; Can, B. Batı Anadolu Senozoyik volkanitlerine ait yeni kimyasal, izotopik ve radyometrik verilerin yorumu. *Turk. Jeoloji Bülteni* **1985**, *28*, 121–136. (In Turkish)
9. Gültekin, A.H.; Örgün, Y. Geochemistry of Andesite-hosted, vein-type Mn-Ba Mineralizations, Bigadiç, Balıkesir, Turkey. *Prog. Min. Oilfield Chem.* **1999**, *1*, 239–248.
10. Gültekin, A.H.; Örgün, Y.; Yavuz, F. Tumanpinarı (Balıkesir-Dursunbey) Fe-Mn cevherleşmesinin jeolojik, mineralojij ve jeokimyasal özellikleri. *Turk. Jeoloji Bülteni* **1998**, *41*, 13–28. (In Turkish)
11. Yigit, O. A prospective sector in the Tethyan Metallogenic Belt: Geology and geochronology of mineral deposits in the Biga Peninsula, NW Turkey. *Ore Geol. Rev.* **2012**, *46*, 118–148. [[CrossRef](#)]

12. Okay, I.A. Tavşanlı zonu: Anatolid-Torid Bloku'nun dalma-batmaya uğramış kuzey ucu. *MTA Derg.* **2011**, *142*, 195–228. (In Turkish)
13. Keten, I. Batı Anadolunun Tectonik Birlikleri. *MTA Derg.* **1966**, *66*, 20–34.
14. Bingöl, E. Batı Anadolunun Jeotektonik evrimi. *MTA Derg.* **1976**, *86*, 14–43.
15. Manav, H.; Gültekin, A.H.; Uz, B. Geochemical evidence for the tectonic setting of the Harmancık ophiolites, NW Turkey. *J. Asian Earth Sci.* **2002**, *24*, 1–9. [[CrossRef](#)]
16. Prelevic, D.M.; Akal, C. Tracking post-collisional dynamics of orogenic mantle in southwestern Anatolia using ultrapotassic mafic rocks as geochemical proxies. In Proceedings of the International Earth Science Colloquium on the Aegean Region, İzmir, Turkey, 1–5 October 2012.
17. Harris, N.B.W.; Kelley, S.; Okay, A.I. Post-collision magmatism and tectonics in northwest Anatolia. *Cont. Min. Petrol.* **1994**, *117*, 214–252. [[CrossRef](#)]
18. Triantaphyllou, M.; Papanikolaou, D. Tectonic change from compression to extension at ±30 Ma in the Thraki Basin (Greece-Turkey). In Proceedings of the International Earth Science Colloquium on the Aegean Region, İzmir, Turkey, 1–5 October 2012.
19. Erentöz, C. *1/500000 Ölçekli Türkiye Jeoloji Haritası*; MTA Genel Müdürlüğü: Ankara, Turkey, 1975.
20. Roedder, E. Technique for the extraction and partial chemical analysis of fluid-filled inclusions from minerals. *Econ. Geol.* **1958**, *53*, 235–269. [[CrossRef](#)]
21. Roedder, E. *Composition of Fluid Inclusion*; U.S. Geological Survey: Reston, VA, USA, 1972; p. 164.
22. Roedder, E. *Fluid Inclusions*; Mineralogical Society of America: Chantilly, VA, USA, 1984; p. 644.
23. Balci, N.; Shanks, W.C.; Mayer, B.; Mandernack, K.W. Oxygen and sulfur isotope systematics of sulfate produced during bacterial and abiotic oxidation of pyrite. *Geochim. Cosmochim. Acta* **2007**, *71*, 3796–3811. [[CrossRef](#)]
24. Schroll, E.; Rantitsch, G. Sulphur isotope patterns from the Bleiberg deposit (Eastern Alps) and their implications for genetically affiliated lead–zinc deposits. *Mineral. Petrol.* **2005**, *84*, 1–18. [[CrossRef](#)]
25. Winchester, J.A.; Floyd, P.A. Geochemical classification of different magma series and their differentiation products using immobile elements. *Chem. Geol.* **1977**, *20*, 325–343. [[CrossRef](#)]
26. Le Maitre, R.W. *A Classification of Igneous Rocks and Glossary of Terms*; Blackwell: Oxford, UK, 1989; p. 193.
27. Leal, P.R.; Correa, M.J.; Ametrano, S.J.; Etcheverry, R.O.; de Brodtkorb, M.K. The manganese deposits of the Pampean Ranges, Arjantine. *Can. Mineral.* **2008**, *46*, 1215–1233. [[CrossRef](#)]
28. Lykasis, N.; Killias, S.P. Epithermal manganese mineralization, Kimolos Island, South Aegean volcanic arc, Greece. In *Bulletin of the Geological Society of Greece*, Proceedings of the 12th International Congress, Patras, Greece, 25 June–1 July 2012; pp. 2646–2656.
29. Haas, J.L. An equation for the density of vapour-saturated NaCl-H₂O solutions from 75–325 °C. *Am. J. Sci.* **1970**, *29*, 489–493. [[CrossRef](#)]
30. Akande, S.O.; Horn, E.E.; Reutel, C. Mineralogy, fluid inclusion and genesis of the Arufu and Akwana Pb-Zn-F mineralization, middle Benue Trough, Nigeria. *J. Afr. Earth Sci.* **1988**, *7*, 167–180. [[CrossRef](#)]
31. Asi, S.M.; Jafari, M.; Sahamiyeh, R.Z.; Shahrokhi, V. Geology, geochemistry, sulfur isotope composition, and fluid inclusion data of Farsesh barite deposit, Lorestan Province. *Iran. Arab. J. Geosci.* **2015**, *8*, 7125–7139.
32. Zou, H.; Zhang, S.; Chen, A.; Fang, Y.; Zeng, Z. Hydrothermal fluid source of the Fengjia Barite-Fluorite Deposit in southeast Sichuan, China: Evidence from Fluid inclusions and hydrogen and oxygen isotopes. *Resour. Geol.* **2016**, *66*, 24–36. [[CrossRef](#)]
33. Nash, J.T. *Fluid Inclusion Studies of Some Gold Deposits in Nevada*; U.S. Geological Survey: Reston, VA, USA, 1972.
34. Sawkins, F.J. *Metal Deposits in Relation to Plate Tectonics*; Springer: New York, NY, USA, 1990; p. 461.
35. Gültekin, A.H.; Örgün, Y.; Suner, F. Geology, mineralogy and fluid inclusion data of the Kızılıcaören Fluorite-barite-REE deposit, Eskişehir, Turkey. *J. Asian Earth Sci.* **2003**, *21*, 365–376. [[CrossRef](#)]
36. Olade, M.A.; Morton, D. Origin of lead-zinc mineralization in the southern Benue Trough, Nigeria-Fluid inclusion and trace element studies. *Miner. Depos.* **1985**, *20*, 76–80. [[CrossRef](#)]
37. Norman, I.D.; Bozrafshan, K.; Eggleston, T.L. Mineralization of the Luis Lopes epithermal manganese deposits in light of fluid inclusion and geologic studies. In *New Mexico Geological Society Guide Book*, Proceedings of New Mexico Geological Society Thirty-Fourth Annual Field Conference, Socorro, NM, USA, 13–15 October 1983; pp. 247–251.

38. Hedenquist, J.W.; Henley, R.W. The importance of CO₂ on freezing point measurements of fluid inclusions: Evidence from active geothermal systems and implications for epithermal ore deposition. *Econ. Geol.* **1985**, *80*, 1379–1406. [CrossRef]
39. Arribas, A.J.R.; Cunningham, C.G.; Rytuba, J.J.; Rye, R.O.; Kelly, W.C.; Podwysocki, M.H.; McKee, E.H.; Tosdal, R.M. Geology, geochronology, fluid inclusions and isotope geochemistry of the Rodalquilar Au alunite deposits, Spain. *Econ. Geol.* **1995**, *90*, 795–822. [CrossRef]
40. Bozkaya, G.; Gökc̄e, A. Lead and sulfur isotope studies of the Koru (Çanakkale, Turkey) lead-zinc deposits. *Turk. J. Earth Sci.* **2009**, *48*, 127–137.
41. Lindgren, W. *Mineral Deposits*; McGraw-Hill: New York, NY, USA, 1933.
42. Cooke, D.R.; McPhail, D.C.; Bloom, M.S. Epithermal gold mineralization, Acupan, Baguio District, Philippines: Geology, mineralization, alteration, and the thermochemical environment of ore deposition. *Econ. Geol.* **1996**, *91*, 243–272. [CrossRef]
43. Ohmoto, H.; Goldhaber, M.B. Sulfur and carbon isotopes. In *Geochemistry of Hydrothermal Ore Deposits*, 3rd ed.; Barnes, H.L., Ed.; Wiley: New York, NY, USA, 1977; pp. 517–611.
44. Rao, D.V.S.; Naqvi, S.M. Geological setting, mineralogy, geochemistry and genesis of the Middle Archaean Kalyadi copper deposit, western Dharwar craton, Southern India. *Miner. Depos.* **1977**, *32*, 230–242. [CrossRef]
45. Bralia, A.; Sabatin, G.F.; Troja, F. A revaluation of the Co/Ni ratio in pyrites as a geochemical tool in ore genesis problems. *Miner. Depos.* **1979**, *14*, 353–374. [CrossRef]
46. Bajvan, Z.; Seccombe, P.K.; Ofter, R. Trace element distribution, Co:Ni ratios and genesis of the Big Cadia iron-copper deposits, New South Wales, Australia. *Miner. Depos.* **1987**, *22*, 292–300.
47. Haas, J.L. The effect of salinity on the maximum thermal gradient of a hydrothermal system at hydrostatic pressure. *Econ. Geol.* **1971**, *66*, 940–946. [CrossRef]
48. Bowers, T.; Helgeson, H. Calculation of the thermodynamic and geochemical consequences of nonideal mixing in the system H₂O-CO₂-NaCl on phase relations in geological systems: Equations of stable H₂O-CO₂-NaCl fluids at high pressures and temperatures. *Geochim. Cosmochim. Acta* **1983**, *47*, 1247–1275. [CrossRef]
49. Yavuz, F.; Gültekin, A.H.; Örgün, Y.; Çelik, N.; Karakaya, M.Ç.; Şaşmaz, A. Mineral chemistry of barium-and titanium-bearing biotites in calc-alkaline volcanic rocks from the Mezitler area (Balıkesir Dursunbey), Western Turkey. *Geochem. J.* **2002**, *36*, 563–580. [CrossRef]
50. Nielsen, H. *Sulfur Isotopes in Isotope Geology*; Jager, E., Hunziker, J.C., Eds.; Springer: New York, NY, USA, 1979; pp. 283–312.
51. Stumbfl, E.F.; Kırıkoğlu, M.S. Fluorite-barite-rare earths deposits at Kızılcaören, Turkey. *Mitt. Österr. Geol. Ges.* **1985**, *78*, 193–200.



© 2016 by the authors; licensee MDPI, Basel, Switzerland. This article is an open access article distributed under the terms and conditions of the Creative Commons Attribution (CC-BY) license (<http://creativecommons.org/licenses/by/4.0/>).